PII: S0955-2219(98)00142-3

0955-2219/98/$—see front matter

Carbon Nanotubes–Fe–Alumina Nanocomposites. Part II: Microstructure and Mechanical Properties of the Hot-Pressed Composites

Ch. Laurent,* A. Peigney, O. Dumortier and A. Rousset

Laboratoire de Chimie des Matériaux Inorganiques, ESA CNRS 5070, Université Paul-Sabatier, F31062 Toulouse cedex 4, France

(Received 20 November 1997; revised version received 7 June 1998; accepted 16 June 1998)

Abstract

Carbon nanotubes–Fe–Al_2O_3 massive composites have been prepared by hot-pressing the corresponding composite powders, in which the carbon nanotubes are arranged in bundles smaller than 100 nm in diameter and several tens of micrometers long, forming a web-like network around the Fe–Al_2O_3 grains. In the powders, the quantity and the quality of the carbon nanotubes both depend on the Fe content (2, 5, 10, 15 and 20 wt%) and on the reduction temperature (900 or 1000°C) used for the preparation. Bundles of carbon nanotubes are present in the hot-pressed materials but with a decrease in quantity in comparison to the powders. This phenomenon appears to be less pronounced for the powders containing higher-quality carbon, i.e. a higher proportion of nanotubes with respect to the total carbon content. The presence of carbon as nanotubes and other species (Fe carbides, thick and short tubes, graphene layers) in the powders modifies the microstructure of the hot-pressed specimens in comparison to that of similar carbon-free nanocomposites: the relative densities are lower, the matrix grains and the intergranular metal particles are smaller. The fracture strength of most carbon nanotubes–Fe–Al_2O_3 composites is only marginally higher than that of Al_2O_3 and are generally markedly lower than those of the carbon-free Fe–Al_2O_3 composites. The fracture toughness values are lower than or similar to that of Al_2O_3. However, SEM observations of composite fractures indicate that the nanotubes bundles, which are very flexible, could dissipate some fracture energy.

*To whom correspondence should be addressed.

1 Introduction

The brittleness of ceramics hampers their use for structural applications. Many strategies have been devised for improving the mechanical properties of ceramics, particularly alumina, notably using dispersions of ZrO_2 particles, SiC whiskers and nanoparticles or metallic micro- or nanoparticles as reinforcing phases. Carbon nanotubes[1] have recently emerged as potentially attractive materials for the reinforcement of ceramics. Indeed, both theoretical and experimental studies[2–7] show that carbon nanotubes have excellent mechanical characteristics. In particular, the Young's modulus of multiwall carbon nanotubes has been calculated[5] to be up to 1·4 times that of a graphite whisker, i.e. about 1 TPa and values derived from thermal vibration experiments performed on several multiwall carbon nanotubes in a transmission electron microscope[7] are in the 0·4–3·7 TPa range. Moreover, the flexibility of carbon nanotubes is remarkable[8] and the bending may be fully reversible up to a critical angle value as large as 110° for single-wall nanotubes.[6]

We have proposed[9] a novel catalytic route for the *in-situ* formation, in a composite powder, of a huge amount of single-wall and multiwall carbon nanotubes, having a diameter between 1·5 and 15 nm and being arranged in bundles that may be up to 100 μm long. The method consists in the selective reduction in H_2–CH_4 atmosphere of an oxide solid solution such as $Al_{1.8}Fe_{0.2}O_3$ or $Mg_{0.9}M_{0.1}Al_2O_4$, (M = Fe, Co, Ni).[9–12] The transition metal particles formed upon reduction are active for the catalytic decomposition of CH_4 and most importantly have a size (< 10 nm) adequate for nanotube nucleation and growth. We have also

proposed[9] a method, based on chemical analysis and specific surface area measurements, that allows to characterize the composite powders at a global level, in terms of both quantity of nanotubes in the powders and quality (high amount of carbon in tubular form and/or small average tube diameter). Indeed, the nanocomposite powders may also contain Fe carbide nanoparticles as well as undesirable thick, short carbon tubes and thick graphene layers covering the Fe/Fe carbide nanoparticles.

The influence of the Fe content and of the reduction temperature on the composition and micro/nanostructure of the carbon nanotubes–Fe–Al_2O_3 powders have been investigated, with the aim of improving both the quantity of nanotubes and the quality of carbon. The results are reported in a companion paper.[13] Briefly, a higher quantity of carbon nanotubes is obtained using α-$Al_{1.8}Fe_{0.2}O_3$ as starting compound, i.e. the maximum Fe concentration (10 cat%) allowing to retain the monophase solid solution. A further increase in Fe content provokes a phase partitioning and the formation of a Fe_2O_3-rich phase which upon reduction produces much larger Fe particles, that appear to favour the formation of thick, short carbon tubes or the deposition of graphene layers at their surface. The higher carbon quality is obtained with only 5 cat% Fe (α-$Al_{1.9}Fe_{0.1}O_3$), probably because the surface Fe nanoparticles formed upon reduction are somewhat smaller than those formed from α-$Al_{1.8}Fe_{0.2}O_3$, thus allowing the formation of carbon nanotubes of a smaller diameter. For a given Fe content ($\leq$10 cat%), increasing the reduction temperature (from 900 to 1000°C) favours the quantity of nanotubes because of a higher CH_4 surpersaturation level in the gas atmosphere, but also provokes a decrease in carbon quality.

The aim of this work is to prepare dense carbon nanotube–Fe–Al_2O_3 materials by hot-pressing the nanocomposite powders and to investigate their microstructure and mechanical properties. The present composites will be compared with carbon-free Fe–Al_2O_3 nanocomposites prepared by the same route which have been found to exhibit higher strength and higher toughness than pure Al_2O_3.[14,15]

2 Experimental

Carbon nanotubes–Fe–Al_2O_3 composite powders have been prepared by selective reduction in H_2–CH_4 gas mixture, at either 900 or 1000°C, of the corresponding oxide powders.[13] The Fe amount was varied so that a total reduction of the Fe^{3+} ions present in the oxide in metallic Fe give composite powders with a metallic phase content equal to 2, 5, 10, 15 and 20 wt%, not taking into account the presence of carbon which varies from one powder to another. For the sake of brevity, the composite powders will be hereafter noted 2R900, 5R900, ..., 20R1000 according to the Fe content and to the reduction temperature. The microstructure of the powders is fairly complex:[13] the Al_2O_3 grains contain a dispersion of nanometric Fe particles, forming a truly nanocomposite matrix. Particles of Fe, Fe–C alloy and Fe carbide (Fe_3C in the R900 specimens and Fe_5C_2 in the R1000 ones) are also located at the surface of the matrix grains, in a proportion that increases with the increase in metal content. These surface particles are either covered by some graphene layers, or connected in some way to a thick, short carbon tube, or connected to an Iijima's-type[1] carbon nanotube. The latter are arranged in bundles smaller than 100 nm in diameter and several tens of micrometers long that form a web-like network around the Fe–Al_2O_3 grains.

The carbon content (C_n), the quantity and the quality of carbon nanotubes in the composite powders depend on both the Fe content and the reduction temperature.[13] As proposed elsewhere,[9] the difference $\Delta S = S_n - S_{on}$ between the specific surface area of the nanocomposite powder (S_n) and that of the same powder after oxidation in air at 850°C (S_{on}) essentially represents the quantity of nanotube bundles in the composite powder. The increase in specific surface area by gram of carbon, $\Delta S/C_n$, can be considered as representing the quality of the nanotubes, a higher figure for $\Delta S/C_n$ denoting a smaller average tube diameter and/or more carbon in tubular form, which we consider a better quality of carbon. These macroscopic characteristics of the carbon nanotubes–Fe–Al_2O_3 powders have been discussed in a companion paper[13] and are presented in Table 1.

The powders were uniaxially hot-pressed in graphite dies, in a primary vacuum, at different temperatures in the 1355–1535°C range depending on the Fe content. The dwell time at the appropriate temperature was fixed to 15 min. The dense specimens (20 mm in diameter and 1 mm thick) for mechanical tests were ground to a finish better than 6 μm with diamond suspensions. Surfaces polished to an optical finish and fracture profiles were observed by scanning electron microscopy (SEM). Densities were calculated from the mass and dimensions of the dense composites. The hot-pressed materials were studied by X-ray diffraction (XRD) with Co K_α radiation ($\lambda = 0{\cdot}17902$ nm). The transverse fracture strength (σ_f) was determined by the three-point-bending test on parallelepipedic specimens ($1{\cdot}6 \times 1{\cdot}6 \times 18\,mm^3$) machined with a diamond blade. The fracture toughness (K_{Ic}) was

Table 1. Some characteristics of the carbon nanotubes–Fe–Al_2O_3 nanocomposite powders[13]

Specimen	C_n *(wt%)*	ΔS *($m^2 g^{-1}$)*	$\Delta S/C_n$ *($m^2 g^{-1}$)*
2R900	0·68	1·25	184
5R900	0·72	1·82	253
10R900	1·64	2·55	155
15R900	5·39	1·73	32
20R900	4·84	1·23	25
2R1000	2·50	1·18	47
5R1000	3·65	3·67	101
10R1000	6·24	4·92	79
20R1000	4·03	0·74	18

C_n: carbon content; ΔS: surface area of carbon for one gram of composite powder, representative of the quantity of nanotubes; $\Delta S/C_n$: specific surface area of carbon, representative of the quality of nanotubes.

measured by the SENB method on similar specimens notched using a diamond blade 0·3 mm in width. The calibration factor proposed by Brown and Srawley[16] was used to calculate the SENB toughness from the experimental results. Crosshead speed was fixed at 0·1 mm min^{-1}. The values given for σ_f and K_{Ic} are the average of measures on seven and six specimens, respectively.

3 Results and Discussion

3.1 Hot-pressing temperature

The composite powders were hot-pressed at different temperatures (Table 2). For a given material, the hot-pressing temperature was fixed at the temperature where no shrinkage was observed anymore on the piston movement sensor. For the R900 powders, the hot-pressing temperature decreases from 1535 to 1355°C when the Fe content is increased from 2 to 20 wt%, revealing the influence of the metal particles. For the R1000 powders, the phenomenon is less pronounced, the hot-pressing temperature decreasing from 1535 to 1455°C when the Fe content is increased from 2 to 20 wt%.

3.2 Density and microstructure

All the measured densities (d_{exp}, Table 2) are lower than the theoretical densities of carbon-free Fe–Al_2O_3 composites (d_{MA}, Table 2), because of the lower density of the carbon species on the one hand and of some remaining porosity on the other hand. A calculation of the theoretical density should take into account the densities and the proportions of the different carbon species. The density of thick, short tubes and the density of the graphene layer deposits can be assimilated to that of graphite (2·25 g cm^{-3}). The density of carbon nanotubes is a function both of their diameter and number of shells. We have calculated that only

Table 2. Hot-pressing temperature and density data

Specimen	T *(°C)*	d_{exp} *(g cm^{-3})*	d_{MA} *(g cm^{-3})*	d_{calc} *(%)*	d_{SEM} *(%)*
2R900	1535	3·86	4·02	97	*d*
5R900	1475	3·82	4·09	94	*dd*
10R900	1450	4·01	4·19	98	*d*
15R900	1425	4·03	4·30	98	*ddd*
20R900	1355	4·01	4·40	95	*dddd*
2R1000	1535	3·77	4·02	96	*dd*
5R1000	1475	3·60	4·09	91	*dd*
10R1000	1475	3·97	4·19	100	*ddd*
20R1000	1455	4·17	4·40	98	*ddd*

d_{exp}: density measured from the mass and dimensions of the dense composite; d_{MA}: theoretical density of the corresponding carbon-free Fe–Al_2O_3 composite; d_{calc}: relative density calculated by assuming that all carbon has the density of graphite, with $d_{graphite} = 2{\cdot}25\ g\ cm^{-3}$; d_{SEM}: qualitative estimation of the relative density evaluated from SEM surface images: *d* denotes a rather poor relative density (about 90–92%) and *dddd* a higher relative density (about 98–100%).

the nanotubes with a small internal diameter ($< 1{\cdot}7$ nm for two shells or < 3 nm for 10 shells) have a density higher than that of graphite. From the diameters and shell number of the nanotubes observed by TEM in previous works,[9,11] we infer that their density is slightly lower than or similar to that of graphite. Thus, with the hypothesis that no carbon is lost during hot-pressing, we have calculated the relative density d_{calc} (Table 2), using the density of graphite (2·25 g cm^{-3}) for all carbon species. The so-obtained d_{calc} are in the 91–100% range.

The SEM secondary electron (SEI) images of polished composites, some of which in Fig. 1, show holes in varying quantities from one specimen to the other. The observation of the images seems to indicate that the 2R900 and the 10R900 composites have the lower relative density whereas the 15R900 and the 20R900 composites have the higher. Thus, using for each composite several images with different magnifications, we have classified the composites from the lower to the higher apparent relative densities (d_{SEM}, labels *d* to *dddd*, respectively), which are in the 90–100% range (Table 2). Some differences appear between d_{SEM} and d_{calc} values. The pull-out of some grains during polishing could account for an under-estimation of d_{SEM} (2 and 10R900, 2 and 10R1000). In addition, a possible insufficient reliability of the d_{SEM} evaluation method could explain the over-estimation for 5R1000 and 20R900. Furthermore, it seems that the hot-pressed composites contain less nanotube bundles than the corresponding powders. As discussed later in this paper, some carbon may be lost during hot-pressing and consequently the relative densities are probably somewhat lower than d_{calc} (Table 2). Thus, it appears that the present nanocomposites including carbon nanotubes are less

densified that similar carbon-free Fe–Al_2O_3 nanocomposites (relative densities in the 97–99% range).[14,15]

Previous works[14,15,17–19] on carbon-free metal–alumina nanocomposites have shown that the metal nanoparticles ($\leq$ 10 nm) located within the matrix grains in the powder remain in intragranular position in the dense material and therefore are protected against excessive growth upon hot-pressing. In contrast, the metal particles located at the surface can coalesce and grow relatively easily up to micronic sizes and are found at the grain boundaries and grain junctions of the matrix. In the present composites, SEM observations of the polished composites show the intergranular Fe (and/or Fe–carbide) particles, appearing in white on the back-scattered electron (BEI) images (some of which shown in Fig. 2). Very few such particles are observed for the 2 wt% Fe composites (2R900 and 2R1000). The number of intergranular particles increases with increasing the Fe content for the composites prepared from both the R900 and R1000 powders, some particles being larger than 1 μm in the 15 and 20 wt% Fe specimens. For a given Fe content, the intergranular particles appear to be smaller in the R1000 than in R900 specimens [Fig. 2]. Interestingly, the intergranular metal particles are always smaller than in similar carbon-free nanocomposites.[14,15,17–19]

Nanotube bundles not larger than 100 nm in diameter and several micrometers long are observed on SEM images of fractures (Fig. 3), but a comparison with images of powders[13] reveals an important decrease in the quantity of bundles. In particular, it seems that the 2 wt% Fe dense composites contain very few bundles. Comparisons between the different massive specimens (images not shown) seem to reveal a higher quantity of bundles in the R900-derived materials than in the R1000-derived ones. This is not what was expected from the results on the powders; indeed, the ΔS values (Table 1) indicated a higher quantity of nanotube bundles in the R1000 powders, notably for 5R1000 and 10R1000 (about twice more). However, it should be noted that $\Delta S/C_n$ values (Table 1) denoted a much lower tube quality in the R1000 powders. It is also noteworthy that nothing comparable to the short, thick tubes present in some powders (15 and 20 wt% Fe)[13] has been observed in the hot-pressed composites.

A low magnification SEI image of the 5R900 specimen [Fig. 3(a)] reveals micrometer-sized matrix grains, and a mixed intergranular–transgranular fracture. It has been shown that the

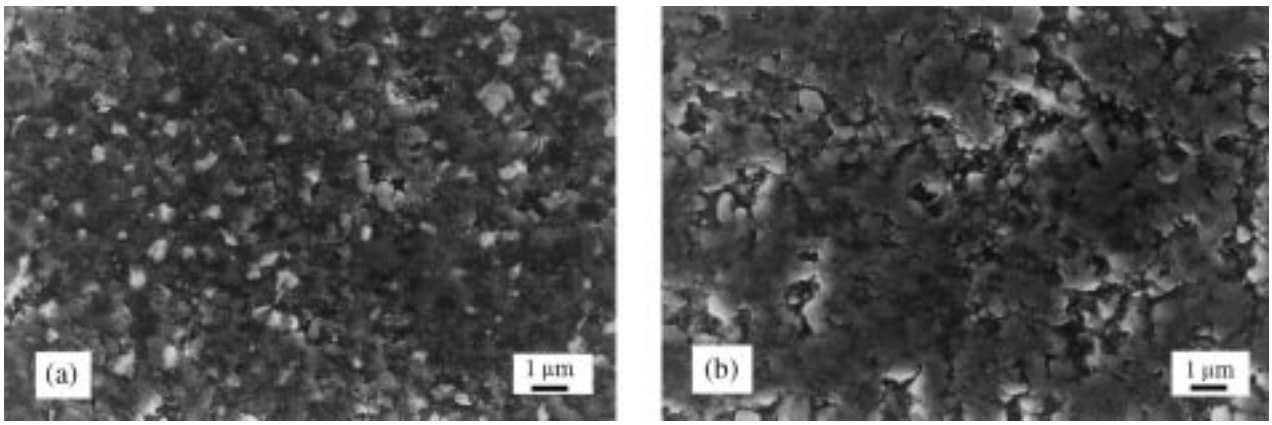

Fig. 1. SEM secondary electron images (SEI) of some polished composites: (a) 20R900, (b) 2R1000.

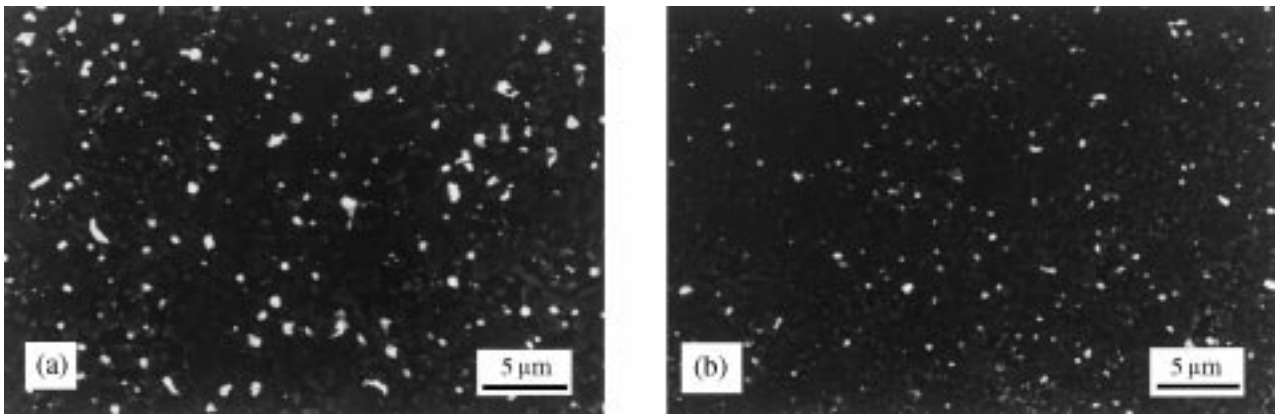

Fig. 2. SEM back-scattered electron images (BEI) of some polished composites: (a) 10R900, (b) 10R1000.

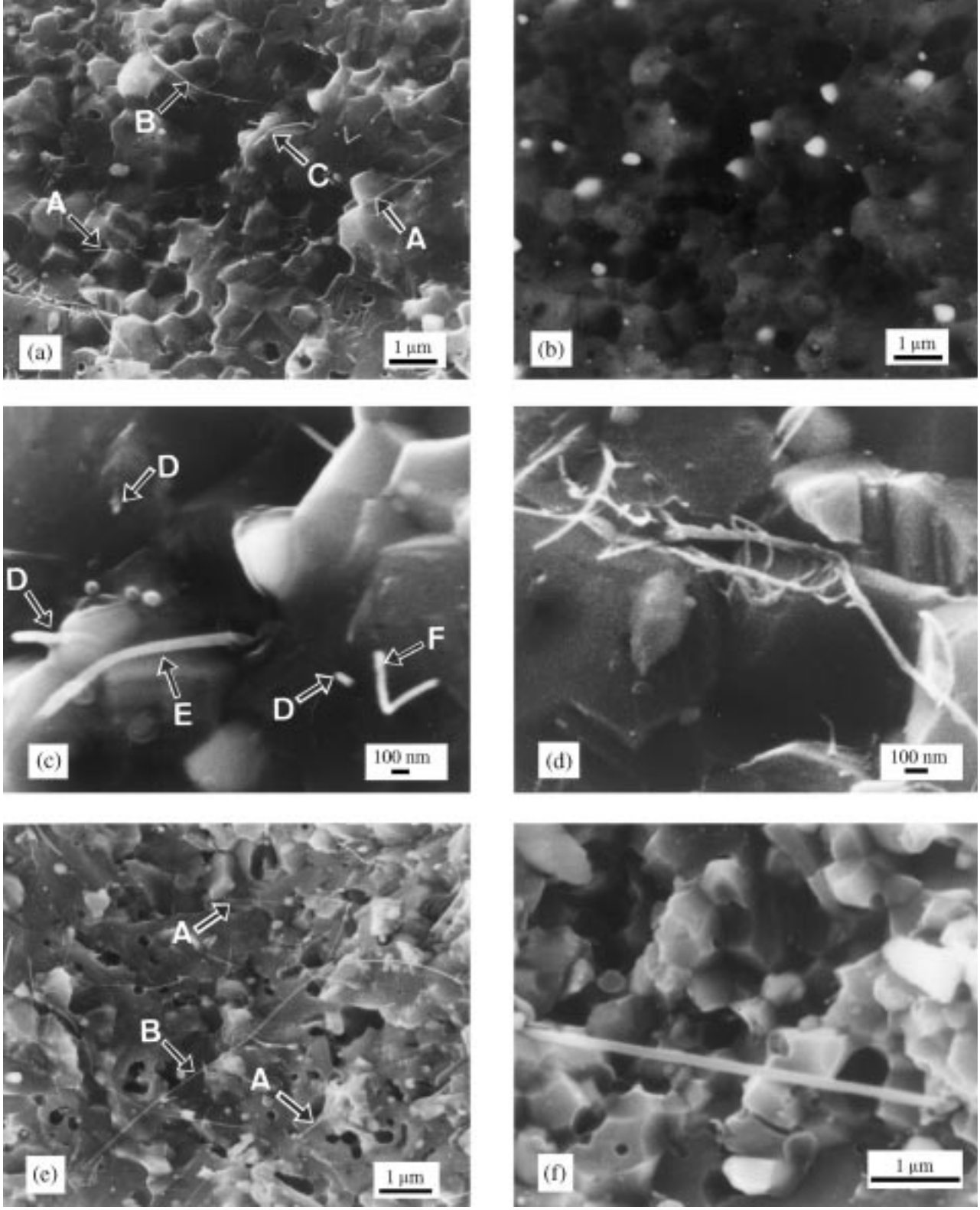

Fig. 3. SEM images of the fracture of some composites: (a–d) 5R900: (a) and (b) are, respectively, SEI and BEI images of the same area; (c) and (d) are details of this area at a higher magnification; (e) 10 R900; (f) 20R900.

intragranular metal nanometric particles promote a transgranular fracture, even for a matrix with a micrometric grain size.[20–23] Some bundles appear to be connected with the matrix at both ends and are either tight (A) or rather slack (B). Some others have been cut during the fracture (C). A BEI image [Fig. 3(b)] corresponding to the same area as the SEI image [Fig. 3(a)] shows the dispersion of Fe (and/or Fe–carbide) particles. One can distinguish two classes of diameters: those in the 200–500 nm range correspond to the intergranular particles and those smaller than 50 nm could be in intragranular position. Figure 3(c) and (d) are higher magnification images of the central part and the lower left

part, respectively, of the area shown in Fig. 3(a). Some bundles (D), which seem to have been entrapped in the matrix grains during hot-pressing, are cut near the grain surface [Fig. 3(c)], suggesting some degree of bundle pull-out. A bundle (E) has been constrained and is bent and another one, at the lower right side of the image (F), has been bent to a very sharp angle. One can observe [(Fig. 3(d)] a bundle that may have been teared up during the fracture, revealing several nanotubes or smaller bundles. The low magnification SEI image of 10R900 [Fig. 3(e)] show similar features than that of 5R900 [Fig. 3(a)] with tight (A) and slack (B) bundles. Note that albeit several images were observed, it was not possible to conclude whether some difference in nanotube bundles quantity exists between the 5 and 10 wt% Fe specimen. In Fig. 3(f), a tight bundle about 100 nm in diameter seems to be embedded between the matrix grains, while the right-hand end looks like it is entrapped in what has been revealed by SEM-BEI observations to be a metal particle, as opposed to a matrix grain.

3.3 X-ray diffraction

Comparing to the patterns recorded on the powders,[13] the patterns of the dense composites prepared from the R900 and R1000 powders show an increase in the α-Fe (110) peak intensity and a decrease in its width, reflecting the growth of the metal particles upon hot-pressing. It seems that less carbides (particularly Fe_5C_2) are present in the dense specimens than in the corresponding powders, showing that hot-pressing in graphite dies does not lead to a carburization of the Fe particles in the present experimental conditions. The intensity of the C_g (002) peak, corresponding to the distance between graphene layers ($d_{002} = 0{\cdot}34$ nm), is similar to that in the powders, but the peak is much clearly resolved owing to a higher a level of crystallization of the graphenic species and because the (012) corundum peak ($d_{012} = 0{\cdot}35$ nm) is more narrow and do not overlap anymore.

3.4 Mechanical properties

The fracture strength and fracture toughness of R900 and R1000 specimens have been measured and are compared with that of Al_2O_3 and Fe–Al_2O_3 nanocomposites prepared by the same route[14,15] (Figs 4 and 5). For the R900 specimens [Fig. 4(a) and (b)], only 5R900 has a fracture strength (553 MPa) significantly higher than that of Al_2O_3 (330 MPa), but lower than that of the corresponding Fe–Al_2O_3 composite (600 MPa). Whatever the Fe content, the fracture toughness is lower than or similar to that of Al_2O_3 (4·4 MPa $m^{1/2}$). The fracture strength of most R1000 specimens

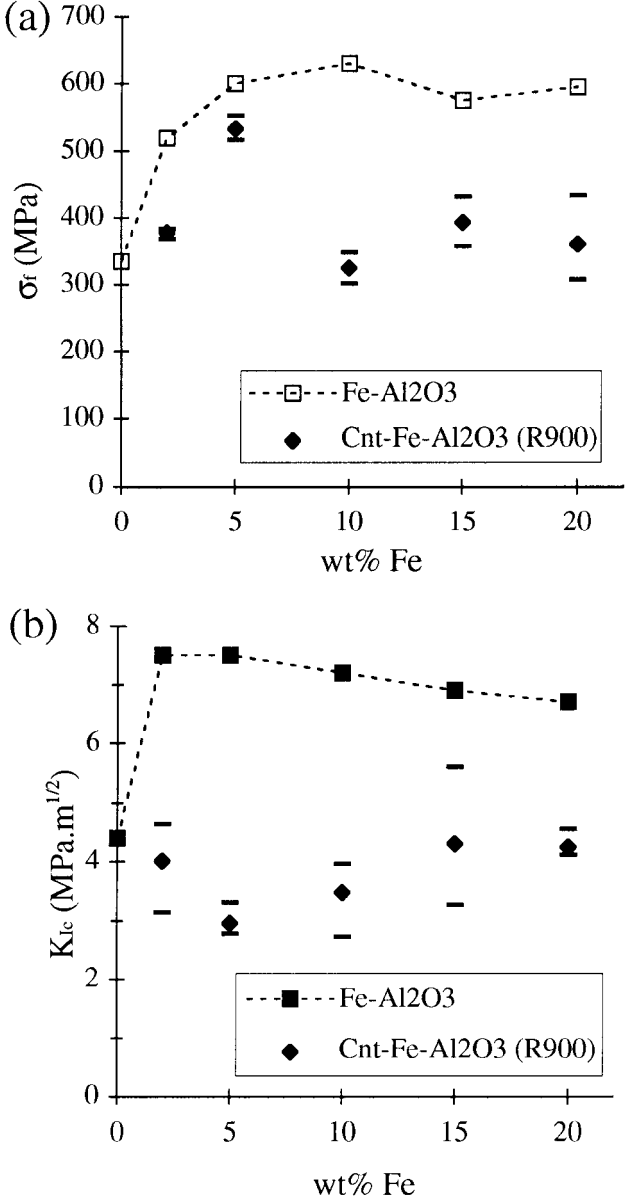

Fig. 4. (a) Fracture strength and (b) fracture toughness of the dense composites prepared from powders reduced at 900°C (◆). The higher and lower measured values are also reported (▭). For the sake of comparison, the values obtained on carbon-free Fe–Al_2O_3 nanocomposites[14,15] are also shown (□). The dashed line is a guide to the eye.

[Fig. 5(a) and (b)] is higher than that of pure Al_2O_3 but it decreases with the increase in Fe content, from 523 MPa for 2R1000 to reach a value equal to that measured for Al_2O_3 (330 MPa) for 20R1000. Except for the 2R1000 composite, the fracture strengths are lower than those of the Fe–Al_2O_3 composites. Whatever the Fe content, the fracture toughness is similar to that of Al_2O_3 [Fig. 5 (b)].

3.5 Discussion

Carbon nanotubes–Fe–Al_2O_3 massive composites have been obtained by hot-pressing the composite powders. However, SEM images (Fig. 3) have revealed an important decrease in the quantity of nanotubes bundles in comparison to the starting

powders. Since this does not correspond to a carburization of the Fe particles, it is proposed that some carbon nanotubes react with residual O_2 to form gaseous carbon species (probably mostly CO). This phenomenon is less pronounced for the R900 than for the R1000 specimen, possibly because the R900 powders contain a higher proportion of nanotubes with respect to the total carbon content (Table 1).

The microstructure of the massive specimens differs from that of similar carbon-free nanocomposites[14,15,17–19] in several respects. Firstly, the relative densities (Table 2) are lower, possibly owing to a detrimental effect of carbon which may inhibit some diffusion processes. Secondly, and probably for the same reason, the matrix grains appear to be twice smaller in the present materials (ca 1 μm versus 2 μm). Thirdly, the Fe (and/or Fe–carbide) particles are smaller (Fig. 2), probably because the graphene layers around them in the present powders[9,11] hamper their coalescence during hot-pressing. This could explain why, for a given Fe content, the intergranular Fe (and/or Fe–carbide) particles appear larger in the R900 than in the R1000 massive composites whereas the surface particles are smaller in the R900 than in the R1000 powders.[13] Indeed, the carbon content is higher and its quality lower in the R1000 powders (Table 1) which could mean that more Fe (and/or Fe–carbide) particles are covered by graphene layers or that the layers are thicker.

It has been shown[22–24] that the hybridization of microcomposites and nanocomposites could result in a further improvement in both the fracture strength and fracture toughness. Obviously, the additive effect that was expected from the hybridization of metal–alumina nanocomposites with very long carbon nanotube bundles is not observed. Indeed, the fracture strength (Figs 4 and 5) of most composites is only marginally higher than that of Al_2O_3 and, except for 5R1000, are all markedly lower than those of the carbon free Fe–Al_2O_3 composites. Similar observations can be made for the fracture toughness values (Figs 4 and 5). This may in part be explained by the presence of residual porosity which will impair the mechanical resistance. No correlation was found between the mechanical properties and the values of ΔS or $\Delta S/C_n$ which represent the quantity and the quality of carbon nanotubes included in the composite, respectively. Comparing with the carbon-free composites, one may also consider that the lower mechanical properties achieved could result from a partial annihilation of the different reinforcement mechanisms: indeed, SEM observations (Fig. 3) show that the fracture is mostly intergranular, while it is essentially intragranular in the absence

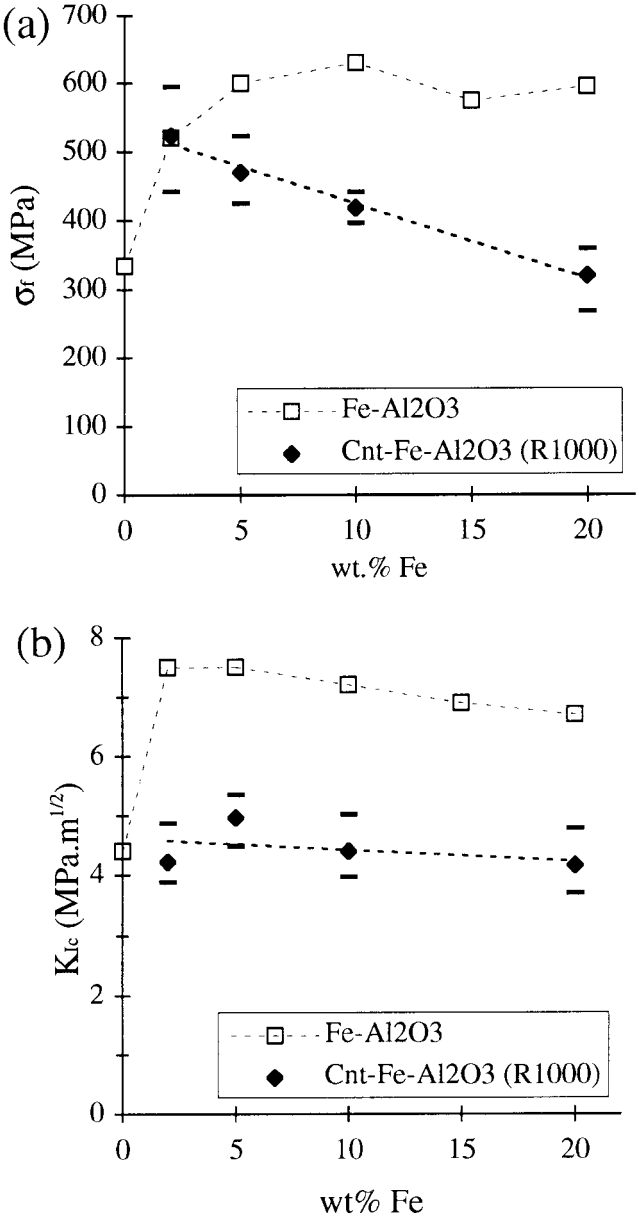

Fig. 5. (a) Fracture strength and (b) and fracture toughness of the dense composites prepared from powders reduced at 1000°C (◆). The higher and lower measured values are also reported (=). For the sake of comparison, the values obtained on carbon-free Fe–Al_2O_3 nanocomposites[14,15] are also shown (□). The dashed line is a guide to the eye.

of carbon.[23,24] Thus, reinforcement mechanisms involving the intragranular metal particles would be far less operative. However, SEM observations of fractures (Fig. 3) seem to indicate that the nanotube bundles could dissipate some fracture energy: some are tight, a few are torn, some others are cut near the matrix surface suggesting some degree of bundle pull-out. The cohesion between the carbon nanotube bundles and the matrix appear to be rather poor, most of them being embedded between the matrix grains. However, some bundles are connected to Fe (and/or Fe–carbide) particles, which should give some cohesion. Possibly the nanotube volume fraction should be greatly

increased and/or carbon nanotube bundles should be aligned or tightened to contribute to the reinforcement.

4 Conclusions

Carbon nanotubes–Fe–Al_2O_3 massive composites have been prepared by hot-pressing composite powders which contain different Fe amounts (2, 5, 10, 15 and 20 wt%) but also different quantity and quality of carbon nanotubes, because these two parameters both depend on the Fe content and on the reduction temperature (900 or 1000°C) used for the powder preparation.[13] Carbon nanotubes have been detected in the hot-pressed materials but with a decrease in quantity in comparison to the corresponding powders. This phenomenon is less pronounced for the R900 than for the R1000 specimen, possibly because the R900 powders contain a higher proportion of nanotubes with respect to the total carbon content. The presence of carbon as nanotubes and others species (Fe–carbides, thick and short tubes, graphene layers) in the powders modifies the microstructure of the hot-pressed specimens in comparison to that of similar carbon-free nanocomposites. Indeed, the relative densities are lower and the matrix grains appear to be twice smaller in the present materials (ca 1 μm versus 2 μm), possibly because carbon may inhibit some diffusion processes. Also, the metal particles are smaller, probably because the graphene layers which cover the Fe (and/or Fe–carbide) hamper the coalescence of these particles during hot-pressing.

In the massive composites, the carbon nanotube bundles, several micrometers long, are not larger than 100 nm in diameter and appear to be remarkably flexible. However, it has not been demonstrated so far that the presence of carbon nanotubes improves the mechanical properties of the composites. Indeed, most fracture strengths of carbon nanotubes–Fe–Al_2O_3 composites are only marginally higher than that of Al_2O_3 and are generally markedly lower than those of the carbon–free Fe–Al_2O_3 composites. Moreover, the fracture toughness values are lower than or similar to that of Al_2O_3. However, SEM observations of composite fractures indicate that the nanotube bundles can dissipate some fracture energy. Work is in progress to prepare composites that could benefit from the properties of the nanotubes, notably by increasing the carbon nanotube volume fraction, improving the relative density of the composites, enhancing the cohesion between the nanotubes bundles and the matrix and giving a preferential orientation to the bundles.

References

1. Iijima, S., Helical microtubules of graphitic carbon. *Nature*, 1991, **354**, 56–58.
2. Calvert, P., Strength in disunity. *Nature*, 1992, **357**, 365–366.
3. Ajayan, P. M., Stephan, O., Colliex, C. and Trauth, D., Aligned carbon nanotube arrays formed by cutting a polymer resin-nanotube composite. *Science*, 1994, **265**, 1212–1214.
4. Ruoff, R. S. and Lorents, D. C., Mechanical and thermal properties of carbon nanotubes. *Carbon*, 1995, **33**, 925–930.
5. Sinnott, S. B., White, C. T. and Brenner, D. W., Properties of novel fullerene tubule structures: a computational study. *Mat. Res. Soc. Symp. Proc.*, 1995, **359**, 241–246.
6. Iijima, S., Brabec, Ch., Maiti, A. and Bernholc, J., Structural flexibility of carbon nanotubes. *J. Phys. Chem.*, 1996, **104**, 2089–2092.
7. Treacy, M. M. J., Ebbesen, T. W. and Gibson, J. M., Exceptionally high Young's modulus observed for individual carbon nanotubes. *Nature*, 1996, **381**, 678–680.
8. Despres, J. F., Daguerre, E. and Lafdi, K., Flexibility of graphene layers in carbon nanotubes. *Carbon*, 1995, **33**, 87–92.
9. Peigney, A., Laurent, Ch., Dobigeon, F. and Rousset, A., Carbon nanotubes grown in-situ by a novel catalytic method. *J. Mater. Res.*, 1997, **12**, 613–615.
10. Peigney, A., Laurent, Ch. and Rousset, A., Synthesis and characterization of alumina matrix nanocomposites containing carbon nanotubes. *Key Eng. Mater.*, 1997, **132–136**, 743–746.
11. Laurent, Ch., Peigney, A. and Rousset, A., Synthesis of carbon nanotubes–Fe–Al_2O_3 nanocomposite powders by selective reduction of different $Al_{1.8}Fe_{0.2}O_3$ solid solutions. *J. Mater. Chem.*, 1998, **8**, 1263–1271.
12. Laurent, Ch., Peigney, A., Quénard, O. and Rousset, A., Novel ceramic matrix nanocomposite powders containing carbon nanotubes. *Key Eng. Mater.*, 1997, **132–136**, 157–160.
13. Peigney, A., Laurent, Ch., Dumortier, O. and Rousset, A., Carbon nanotubes–Fe–alumina nanocomposites. Part I: influence of the Fe content on the synthesis of powders. *Journal of the European Ceramic Society*, 1998, **18**(14), 1995–2004.
14. Devaux, X., Laurent, Ch., Brieu, M. and Rousset, A., Ceramic matrix nanocomposites. In *Composites Materials*, ed. A. T. Di Benedetto, L. Nicolais and R. Watanabe. Elsevier Science, Amsterdam, 1992, pp. 209–214.
15. Rousset, A., Alumina–metal (Fe, Cr, $Fe_{0.8}Cr_{0.2}$) nanocomposites. *J. Sol. State Chem.*, 1994, **111**, 164–171.
16. Brown, W. F. and Srawley, J. E., *Plane Strain Crack Toughness Testing of High Strength Metallic Materials*. ASTM Spec. Tech. Pub., 410, ASTM, Philadelphia, PA, 1966.
17. Laurent, Ch., Devaux, X., Brieu, M. and Rousset, A., Microstructural and mechanical properties of alumina–iron–chromium alloys nanocomposites. In *Euro-Ceramics II*, ed. G Ziegler and H. Hausner. Deutsche Keramische Gesellschaft e.V., Köln, 1992, pp. 1679–1683.
18. Devaux, X., Laurent, Ch., Brieu, M. and Rousset, A., Propriétés microstructurales et mécaniques de nanocomposites à matrice céramique. *C. R. Acad. Sci. Paris Série II*, 1991, **312**, 1425–1430.
19. Laurent, Ch., Devaux, X. and Rousset, A., Elaboration and properties of metal–alumina nanocomposites. *J. High Temp. Chem. Proc.*, 1994, **3**, 489–505.
20. Sekino, T., Nakahira, A., Niihara, K. and Nawa, M., Fabrication of Al_2O_3/W nanocomposites. *KONA Powder and Particle*, 1992, **10**, 192–197.
21. Sekino, T., Nakahira, A., Nawa, M. and Niihara, K., Fabrication and mechanical properties of tungsten metal dispersed Al_2O_3 based nanocomposites. In *Proceedings of*

the International Conference Ceramics Adding the Value: Austceram 92, ed. M. J. Bannister. CSIRO, Australia, 1992, pp. 745–750.
22. Niihara, K., Nakahira, A. and Sekino, T., New nanocomposite structural ceramics. *Mat. Res. Soc. Symp. Proc.*, 1993, **286**, 405–412.
23. Laurent Ch., Contribution à l'étude de nanocomposites a matrice céramique. Alumine–alliages fer–chrome et alumine–zircone–fer et alliages fer–chrome. Doctoral thesis, Université Paul-Sabatier, Toulouse, France, 1994.
24. Laurent Ch., Rousset and A., , Metal–oxide ceramic matrix nanocomposites. *Key Eng. Mater.*, 1995, **108–110**, 405–422.